RESEARCH ARTICLE

An Improved Medical Image Compression Method Based on Wavelet Difference Reduction

MATINA C. H. ZERVA[1], VASILEIOS CHRISTOU[2], NIKOLAOS GIANNAKEAS[2], ALEXANDROS T. TZALLAS[2], AND LISIMACHOS P. KONDI[1], (Senior Member, IEEE)
[1]Department of Computer Science and Engineering, University of Ioannina, 45110 Ioannina, Greece
[2]Department of Informatics and Telecommunications, University of Ioannina, 47100 Arta, Greece

Corresponding author: Alexandros T. Tzallas (tzallas@uoi.gr)

ABSTRACT Advanced microscopic techniques such as high-throughput, high-content, multispectral, and 3D imaging could include many images per experiment requiring hundreds of gigabytes (GBs) of memory. Efficient lossy image-compression methods such as joint photographic experts group (JPEG) and JPEG 2000 are crucial to managing these large amounts of data. However, these methods can get visual quality with high compression ratios but do not necessarily maintain the medical data and information integrity. This paper proposes a novel and improved medical image compression method based on color wavelet difference reduction. Specifically, the proposed method is an extension of the standard wavelet difference reduction (WDR) method using mean co-located pixel difference to select the optimum quantity of color images that present the highest similarity in the spatial and temporal domain. The images with large spatiotemporal coherence are encoded as one volume and evaluated regarding the peak signal-to-noise ratio (PSNR) and structural similarity index (SSIM). The proposed method is evaluated in the challenging histopathological microscopy image analysis field using 31 slides of colorectal cancer. It is found that the perceptual quality of the medical image is remarkably high. The results indicate that the PSNR improvement over existing schemes may reach up to 22.65 dB compared to JPEG 2000. Also, it can reach up to 10.33dB compared to a method utilizing discrete wavelet transform (DWT), leading us to implement a mobile and web platform that can be used for compressing and transmitting microscopic medical images in real time.

INDEX TERMS Imaging, microscopy, image compression, color wavelet difference reduction.

I. INTRODUCTION

Medical image compression has become a prevalent tool with a significant impact on diagnosing diseases in clinical practice [1]. The problem of compressing and transmitting an image in real-time, given the bandwidth of the communication channel, is of great importance, especially in a low-speed connection environment. This problem is not easy to solve because medical images typically contain a huge amount of important diagnostic information, so distortion is not allowed [2]. Real-time constraints limit image compression applications for transmission purposes. On the other hand, image compression applications for storage purposes are less stringent since most algorithms are not executed in real time.

The associate editor coordinating the review of this manuscript and approving it for publication was Chao Zuo.

There is a wide variety of image transform-based coding techniques, which amongst others, are based on discrete cosine transform (DCT) and discrete wavelet transform (DWT) [3]. The DCT method proposed by Nasir [4] transforms image pixels from the spatial domain into the frequency domain, allowing redundancy to be found. The Hungarian mathematician Alfréd Haar created the first DWT method. The main characteristic of this method is that the wavelets are discretely sampled, and it has a temporal resolution that allows capturing both frequency and location information [5].

Regarding compressing volumetric medical datasets, it appears that three-dimensional (3D) wavelet-based encoders outperform DCT-based solutions while providing the required functions such as quality scaling, resolution, random access, and region coding [6]. Narmatha et al. [7] proposed a two-stream method for encoding and decoding medical images by dividing and merging different regions of

the wavelet subbands. Amri et al. [8] created three medical image compression approaches by combining image reduction and expansion techniques, digital watermarking, and different lossless compression standards into a single processing pipeline. The lossless compression standards included the joint photographic experts group lossless standard (JPEG-LS) and the tag image file format (TIFF).

In recent years, much effort has been paid to volumetric medical image compression, where 3D medical images can be viewed as time sequences or volume tomographic slices of an object. Bruylants et al. [9] employed the wavelet transformation to allow support for volumetric image datasets. Ravichandran et al. [10] have also used the wavelet transform to compress 3D medical images. Based on the fact that most medical images are being captured in hospitals and medical organizations using two-dimensional (2D) and 3D monitoring techniques, their simulation results have shown that 3D medical images have high-frequency patterns. Therefore, the waveform technique allows higher peak signal-to-noise ratio (PSNR) values even at the highest compression ratio than 2D medical images. Senapati et al. [11] proposed the 3D hierarchical listless block (3D-HLCK) algorithm, a modified 3D block coding algorithm containing a listless variant. Tang and Pearlman [12] created the 3D set partitioning embedded block method (3D-SPECK), which encodes 3D volumetric image data by utilizing the dependencies in each dimension. Chen et al. [13] developed an end-to-end learning-based framework for 3D volumetric image compression. The framework uses the intra-slice and inter-slice information to predict the entropy coding distribution. Also, it utilizes two novel gating mechanisms for better aggregation of the intra-slice and inter-slice features. Nagoor et al. [14] proposed a lossless compression algorithm that trains a neural network as a 3D data predictor for medical image volumes containing images with 65,536 levels of colors and tones.

Additionally, Zerva et al. [15] proposed an extension of the standard wavelet difference reduction (WDR) method using mean co-located pixel difference (MCPD) to select the optimal number of slices that exhibit the highest similarity in the spatial and temporal domain. The slices with large spatiotemporal coherence are encoded together as one volume in terms of higher PSNR and structural similarity index (SSIM). It is found that the perceptual quality of the medical image is remarkably high. The results indicate that the PSNR improvement over existing schemes may reach up to 3.8 dB and can guide us to implement a mobile and web platform that can be used for compressing and transmitting medical images in real-time.

According to our knowledge, the compression of microscopic images using set partitioning methods has not been tried yet. Color pictures display more information than grayscale images since color pictures display the same number of grayscale tones as in grayscale images plus a number of colors on every image, thus, improving contrast resolution. From a medical point of view, color images disclose important information, which can be critical for diagnostic

purposes. Therefore, it motivated us to propose an extension of the original WDR method to effectively compress microscopic images, namely color wavelet difference reduction (CWDR).

Our main contribution is designing a medical image compression method that can be easily reproduced. It is suitable for use in various color medical images of big sizes, such as microscopic images. It achieves state-of-the-art compression results with a high compression ratio and small information loss within an acceptable range. Extensive evaluations have been performed in a custom-created dataset containing image data extracted using the Hamamatsu NanoZoomer 210. The dataset contained 31 slides of colorectal cancer, and the proposed CWDR algorithm achieved high compression ratios in all images while maintaining high visual quality.

II. RELATED WORK

Current practice in the medical image compression field is to reduce the size of medical image files by reversible (lossless) [16] compression, which offers up to 3 times size reduction, or irreversible (lossy) [17] compression. Irreversible compression allows for a much larger (between 8 and 25 times) size reduction without significant loss of visual quality of the material.

There are many irreversible standards used for compressing images. One of the most popular ones for medical applications is the standard from joint photographic experts group (JPEG) [18]. The vital feature of JPEG is that it enables compression at various levels, thus allowing the user to choose the quality of the compressed image so that information losses are not visible to physicians. JPEG 2000 [19] is the successor of the JPEG standard that provides compression with no or very little information loss, so the image quality does not deteriorate but approximates the image quality without compression. Compared to the JPEG standard, the JPEG 2000 standard provides a typical compression gain of 20% on average, depending on the image features. In low-bitrate applications, studies have shown that JPEG 2000 is superior to H.264 intra-coding [20].

Among reversible compression algorithms, Huffman coding is one of the oldest methods of compressing image data. Developed by Huffman [21], it is used to reduce coding redundancy without degrading the quality of the reconstructed image. Other reversible compression algorithms are arithmetic coding and lossless predictive coding. Arithmetic coding converts a string of data symbols to a code string that can be decoded back to the original data using an encoding and decoding algorithm. Arithmetic coding is a group of codes having the same property of considering the code string as a magnitude [22]. Lossless predictive coding is a two-stage approach that utilizes a lossless adaptive predictor followed by arithmetic coding [23].

Recent lossless approaches involve the multi-dimensional compression by substring enumeration (MCSE) by Dubé [24]. CSE is a compression algorithm for bit strings

FIGURE 1. General elements of an irreversible compression technique. An irreversible compression technique is, in general, a three-stage process. The procedure begins by decomposing or transforming the image, followed by a quantization and symbol encoding process.

that was generalized to higher dimensions to handle all types of images. Makarichev et al. [25] modified the irreversible discrete atomic compression (DAC) algorithm by adding compressed data describing the difference between the original image and the compressed one inside the corresponding DAC file. The addition combined with the compressed image results in a reconstructed image without any distortions. Lee et al. [26] developed a high-throughput image-compression technique using the Golomb-Rice coding and its hardware architecture. Descampe et al. [27] proposed the JPEG XS compression algorithm for visually lossless, low-latency lightweight image coding. It is an international standard that achieves similar (slightly lower) compression ratios compared to JPEG 2000 method. One advantage over JPEG 2000 is that it consumes significantly less power and requires fewer logic resources in hardware implementations.

A significant number of approaches utilize artificial neural networks (ANNs) for specific tasks to increase the compression ratio. Min et al. [28] created a hybrid approach to compress three-dimensional (3D) medical images. The hybrid algorithm utilizes the medical images' anatomical features to divide the medical data into specific areas. Then, a deep neural network creates optimal predictors in each area. The predictors can be switched adaptively according to the area's characteristics being compressed. Finally, the residuals are compressed using an entropy coding scheme. Yang et al. [29] created an image compression-encryption algorithm with the help of a fractional-order memristive BPF chaotic circuit and a back-propagation (BP) trained neural network. The neural network compresses the image while the encryption process is done using a zigzag algorithm with a xor operation. Rhee et al. [30] created a lossless compression technique based on the multi-layer perceptron (MLP) neural network. The MLP outputs prediction errors and contexts which are introduced as input to adaptive arithmetic encoders. Zhu et al. [31] used a long short-term memory (LSTM) neural network for building a predictor, which is used in lossless compression.

In contrast, among the irreversible compression algorithms (created by the need to produce significantly lower bit rates), there are various approaches to lossy image compression, such as vector quantization, coding prediction [32], and transform coding. The general components of a lossy image compression technique involve the three stages (decomposition or transformation, quantization, and symbol encoder) shown in Fig. 1.

There are various transformations used in image compression. The Karhunen-Loève transform (KLT) [33], [34], [35] is an orthogonal linear transformation technique which removes pairwise statistical correlation amongst the transform coefficients. The piecewise Fourier transform (PFT) [36] can maintain image quality by compressing the images' bandwidth. The discrete Walsh-Hadamard transform (DWHT) [37], [38] is an orthogonal transformation type that breaks down a signal into a series of Walsh functions (orthogonal and rectangular wave-forms). Finally, the wavelet transform algorithms [39], which have prevailed in the compression of medical images, are used as frequency analysis and signal coding tools in complex non-stationary signals.

Recent irreversible compression algorithms include the work of Xu et al. [40], which improved the singular value decomposition (SVD) method using a singular vector sparse reconstruction strategy. Guo et al. [41] developed an image compression framework for computer vision applications in embedded systems. The framework makes use of the trade-off between memory traffic and vision performance. Sadchenko et al. [42] created a compression algorithm based on the samples decimation method for medical images, which considers medical image peculiarities.

Some lossy approaches utilize ANNs to increase the compression ratio. Dua et al. [43] used a convolutional neural network (CNN) for compressing hyperspectral images. The algorithm combines CNN's auto-encoder, convolution, and max-pooling layers to reduce the image's dimensions and produce a compressed image. The image can be restored with some loss of information by reversing the CNN's steps using the CNN's decoder and transpose convolution layer. Zhao et al. [44] utilized multiple description CNNs to compress images for transmission. Multiple description coding (MDC) is used for signal transmission in unreliable and non-prioritized networks. Mishra et al. [45] proposed a two-stage auto-encoder-based framework for compressing and decompressing malaria red blood cell images. The above irreversible methods managed to get high compression ratios, but they are unsuitable for medical images since they can lose potentially valuable medical information.

III. MEDICAL IMAGE COMPRESSION EVALUATION METHODS

Several methods evaluate the clinical acceptance of the compression level [46]. The first is the numerical analysis of the pixel before and after compression [47]. This simple method is recommended for calculating the mean pixel error for the compressed image but has no correlation with radiologists' evaluations and therefore has no clinical significance. A second method uses a subjective observer to evaluate with a focus on visual acceptance and presumptive diagnostic value. Many approaches have been proposed, including image scores from the least to the most compressed or subjective evaluations of the onset of a pathological process. None of this leads to reliable and reproducible results. A third

method is the objective measurement of diagnostic accuracy using blind method evaluation. This category of methods is the most reliable.

The relationship between "optically lossless" compression and "diagnostically lossless" is complex. There is evidence that despite the apparent visual degradation from compression, high performance equivalent to that of uncompressed images for certain details, body parts, and diagnostic methods can be achieved. This equivalent does not alter the ability of a radiologist to successfully interpret a poor-quality image (perhaps with less confidence). On the other hand, many physicians are reluctant to interpret compression-degraded images, so the "visually lossless" limit may be the limiting factor despite the "diagnostically lossless" limit, assuming that the former implies less compression than that. Conversely, although it is often assumed that if there is no visual quality loss, there can be no diagnostic loss. The above claim has not been sufficiently investigated, and there is a possibility that the experimental way which defines the thresholds for visual perception without losses is insufficient to guarantee diagnostic performance. Challenging tasks, including low-contrast detection, must maintain high-frequency information, or they will be vulnerable to high compression rates, which are misinterpreted as false-positive findings [48].

Simple mathematical measurements that quantify the difference between the original and the decompressed image, such as PSNR and mean square error (MSE), are poorly correlated with visual or diagnostic performance, and more advanced measurements have been developed. SSIM [49] is a method for measuring the similarity between two images. The SSIM index can be considered a measure of the quality of one of the images being compared, provided that the other image is considered of excellent quality. Another method based on mathematical models simulates human physiology. These software tools could help measure image similarity or differences and determine noticeable difference (JND), signal-to-noise ratio (SNR) ratios, or levels. Probability for detecting differences in the number of pixels. Here, the structural similarity method (SSIM) is an improvement over traditional methods such as PSNR and MSE because it appears to be more consistent with HVS performance [50].

The amount of "information" in an image is described as its "entropy." which can be estimated mathematically, with varying degrees of complexity. A simple measure is the zero-order entropy (sum of the environmentally independent probabilities of each pixel value). The degree to which an image can be compressed using reversible compression can also be used as a measure of entropy. An image's entropy determines its compression ratio before the difference is visually or diagnostically detectable. A significant factor in a medical image's entropy is the amount of rectangular pixel panel occupied by the body part (e.g., consider a small versus a large breast on a fixed-size mammography scanner). Also important is the amount of noise in any unstable background (non-static) or area that has been separated [51].

High entropy images should probably be processed with lower compression ratios to irreversible compression than those with more uniform content. A simple approach is to measure the file output size of a reversible image compression method (JPEG lossless or JPEG 2000), which should be larger for images with higher entropy. Other reliable methods, such as image compositional complexity (ICC), fractal dimension (FD), or region of interest (ROI), may be more effective at computing and creating images. more noise resistant [52].

IV. WAVELET TRANSFORM

The wavelet transform combines low-pass and high-pass filtering into a spectral signal decomposition and extremely fast implementation. Before considering the wavelet transformations of 2D images, it is useful first to consider the wavelet transformations of one-dimensional (1D) signals [53], [54]. Given a 1D signal $s_0[n]$, its 1-level wavelet transform is the mapping $s_0[n] \rightarrow (s_1[2n]|d_1[2n])$ defined by the formulas (1) and (2).

$$s_1[2n] = \sum_{k=-M}^{M} a_k s_0[2n+k] \qquad (1)$$

$$d_1[2n] = \sum_{k=-N}^{N} \beta_k s_0[2n+k+1] \qquad (2)$$

The signals $s_1[2n]$ and $d_1[2n]$ are respectively low-pass and high-pass filterings of $s_0[n]$. These filterings have also been down-sampled and are defined over the indices $\{2n\}$ rather than $\{n\}$. Viewed as sampled, signals are sampled at half the rate as s_0. The coefficients $\{a_k\}$ are the low-pass coefficients and the coefficients $\{\beta_k\}$ are the high-pass coefficients [53].

These coefficients have some basic properties which are shared by other wavelet systems. One important property is that they define an invertible transform. Perhaps just as importantly, the high-pass coefficients satisfy $\sum \beta_k = 0$ and $\sum k\beta_k = 0$. Consequently, if s_0 is linear (or approximately linear) over the indices $2n, 2n+1, 2n+2$, then $d_1[2n] = 0$ (or $d_1[2n] \approx 0$). When s_0 is obtained from samples of a piecewise smooth function, the high-pass filtering d1 will be essentially zero-valued (except near transitions between pieces of the piecewise smooth function). This provides the foundation for compression. When the transform $s_m \rightarrow (s_{m+1}|d_{m+1})$ is iterated on the low-pass outputs $s_1, s_2, \ldots$, then many levels of transformation will produce large numbers of zero values (or almost zero values) at high-pass outputs $d_2, d_3, \ldots$ Such high redundancy of zero values, in $d_1, d_2, d_3, \ldots$, allows for significant compression [53].

A wavelet transform for 1D signals can easily be generalized to 2D images by applying it separately to each dimension. The first level of a discrete particle transformation of a matrix $F = J \times K$, where J and K are both even, is obtained in a two-step manner. The first step can be seen in equation (3) and involves transforming each row of F with a 1D particle

WDR Encoding

Source Image → Wavelet Transform → WDR Encoder → Compressed Bits

WDR Decoding

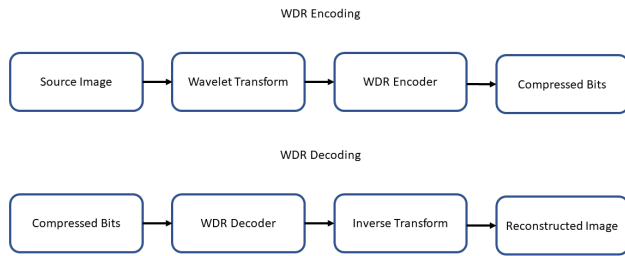Compressed Bits → WDR Decoder → Inverse Transform → Reconstructed Image

FIGURE 2. WDR block diagram. The encoding step of the WDR algorithm involves importing an uncompressed image that undergoes a wavelet transformation phase. Then, it is sent as input to the WDR encoder, which produces the compressed image's bits. The reconstructed image is produced by importing the compressed image bits to the WDR decoder. The decoded data undergo an inverse transform procedure, producing the final reconstructed image.

transformation by taking a matrix $\tilde{F}$.

$$F \rightarrow \begin{pmatrix} s_1^1 | d_1^1 \\ s_2^1 | d_2^1 \\ \vdots \\ s_j^1 | d_j^1 \end{pmatrix} \tag{3}$$

The second step, shown in formula (4) transforms each column of $\tilde{F}$ by the same 1D transform where A^1, V^1, H^1, and D^1 are each $\frac{J}{2} \times \frac{K}{2}$ sub-matrices. Steps one and two are independent and may be performed in either order [53].

$$F \rightarrow \left(\frac{A_1^1 | V_1^1}{H^1 | D^1} \right) \tag{4}$$

The wavelet transform can be iterated on the row-low-pass/column-low-pass outputs (two-level transform). Doing this on A^1 produces submatrices A^2, V^2, H^2, and D^2. As with 1D signals, the second level sub-matrices are responses to the 2D image values having twice the range of pixels (twice the scale) as the first level sub-matrices [53].

V. THE WDR METHOD

The WDR algorithm follows the basic concepts of the set partitioning in hierarchical trees (SPIHT) algorithm by incorporating extra features that aggregate the coefficients to an area of interest (Fig. 2). By reducing the difference between the wavelet coefficients, it recognizes the important wavelet coefficients and improves their accuracy to achieve high compression ratios. During WDR encoding, the generated compressed output consists of the most important coefficients and the sequence of bits, which briefly describe the exact position of the significant values. It offers good perceptual quality and a high compression rate while maintaining the edges of the image. It is suitable for compressing low-resolution medical images at a low bit rate per pixel [55].

The WDR algorithm consists of five parts, as shown in Fig. 3. In the Initialization section, an initial threshold value of T_0 is selected so that all transform values are less than T_0 and at least one is greater than or equal to $T_0 = 2$. The

Initialize → Threshold/2 → Significance Pass → Refinement Pass

FIGURE 3. WDR compression diagram. The WDR algorithm initially calculates the image's DWT, then classifies the particle transformation coefficients from the largest scale to the finest scale and sets an initial T-threshold. The next steps are the significance pass and the refinement pass. The latter gets the improvement values from all significant factors except those found in the classification step of the current iteration round. Finally, the loop divides the threshold by two and repeats the process from step 2.

purpose of the loop indicated in Fig. 3 is to encode significant transformation values by the bit-level encoding method. In relation to the quantity T_0, a binary expansion is calculated for each transformed value. The loop is the process by which these binary extensions are calculated. As the threshold is halved, the significance pass and refinement pass calculate the next bit.

The general model of the WDR method is shown in the following distinct steps of the algorithm.

- Initialize: Calculate the DWT of the original image
- Threshold/2: Classify the particle transformation coefficients from the largest scale to the finest scale and set an initial T threshold.
- Significance pass: Find the significant coefficients' positions relative to the T-threshold and export these significant coefficients.
- Refinement pass: Get the improvement values of all significant factors, except those found in the classification step of this iteration round.
- Loop: Divide the threshold T by two and go to step 2.

Specifically, each step of the WDR algorithm can be seen in Algorithm 1.

The WDR method is equipped with a built-in encoding scheme that can achieve any compression ratio and is competitive with other image compression algorithms

VI. THE CWDR METHOD

The family of set partitioned methods was initially designed for grayscale image compression. To apply them to color images, we must first understand color space. The color image is usually in RGB format. The RGB color spaces are highly correlated, so transformation to a less correlated space is required for efficient lossy compression. The original RGB images were transformed using standard transformations to code the YC_bC_r color space such that the luminance channel Y is stored as one byte for each pixel. On the other hand, the two chrominance channels are stored as one byte for each block of, say, $n \times n \times n$ pixels, i.e., Cb and Cr are the blue component and red component related to the chroma component.

The proposed method, CWDR, is an extension of WDR for color images. This method compresses each color plane at the coding stage and generates three separate bitstreams of the same bitrate. Then, the generated bitstream of each color

Algorithm 1 : The WDR Method

Step 1: (Initialize). Choose an initial threshold T_0 so that all transform values satisfy $|x_m| < T_0$ and at least one transform value satisfies $|x_m| \geq \frac{T_0}{2}$

Step 2: (Update threshold). Let $T_k = \frac{T_{k-1}}{2}$

Step 3: (Significance pass). Perform the following procedure while scanning through insignificant values for higher thresholds

1: Initialize step counter $C = 0$
2: Let $C_{old} = 0$
3: **repeat**
4:     Get next insignificant index m
5:     Increment step-counter C by 1
6:     **if** $|x_m| \geq T_k$ **then**
7:         Output sign x_m and set $q_m = sgn(x_m) \cdot T_k$
8:         Move m to the end of significant indices sequence
9:         Let $n = C - C_{old}$
10:       **if** $n > 1$ **then**
11:          Output reduced binary expansion of n
12:       **else if** $|x_m| < T_k$ **then**
13:          Let q_m retain its initial value of 0
14:       **end if**
15:     **end if**
16: **until** end of insignificant indices
17: Output end-marker
18: The end-marker is a plus sign followed by the reduced binary expansion of $n = C + 1 - C_{old}$ and a final plus sign

Step 4: (Refinement pass). Scan through significant values found with higher threshold values T_j, for $j < k$ (if $k = 1$ skip this step). For each significant value x_m, do the following

19: **if** $|x_m| \in [|q_m|, |q_m| + T_k]$ **then**
20:     Output bit 0
21: **else if** $|x_m| \in [|q_m| + T_k, |q_m| + 2T_k]$ **then**
22:     Output bit 1
23:     Replace value of q_m by $q_m + sgn(q_m) \cdot T_k$
24: **end if**

Step 5: (Loop). Repeat steps 2 through 4 (exiting at any point if bit budget is exceeded)

FIGURE 4. System Flowchart.

space would be serially concatenated. The proposed system structure flowchart is shown in Fig. 4 while its algorithmic structure can be seen in Algorithm 2. The operation starts by selecting suitable colors and image scales. The next step represents the application of variable filters of the wavelet transforms. Then, some quantization processes are performed to show the elements of a big set in terms of a smaller set to lower the number of bits necessary to indicate all possible values of mapping outputs to fewer bits.

In the RGB color model, a color image can be represented by the following intensity function.

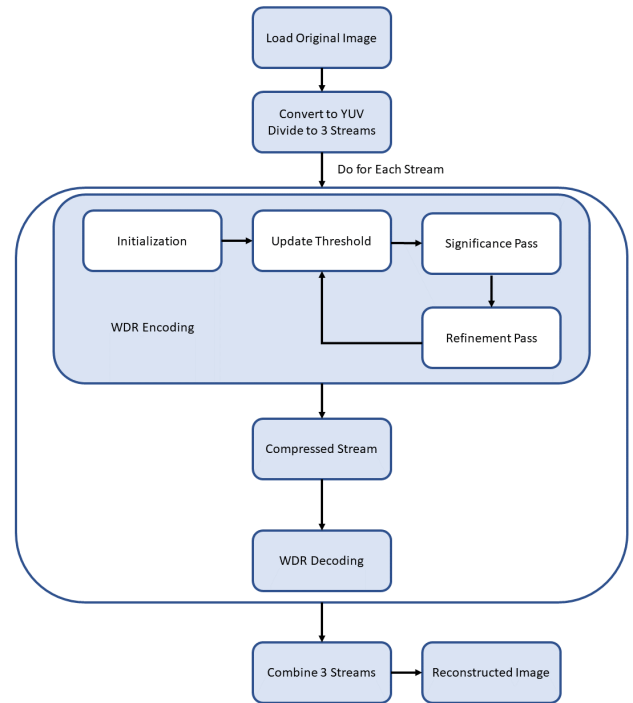$$I_{RGB} = (F_R, F_G, F_B) \qquad (5)$$

where $F_R(x, y)$ is the intensity of the pixel (x, y) in the red channel, $F_G(x, y)$ is the intensity of pixel (x, y) in the green channel, and $F_B(x, y)$ is the intensity of pixel (x, y) in the blue channel. The intensity of each color channel is usually stored using eight bits, which indicates that the quantization level is 256. That is, a pixel in a color image requires total storage of 24 bits. A 24 bit memory can express $2^{24} = 16777216$ distinct colors. The number of colors should adequately meet the display effect of most images. Such images may be called true color images, where each pixel's information is kept using a 24-bit memory.

To split the RGB image into three streams, we separately save each channel to different variables as seen in (6).

$$\begin{bmatrix} R \\ G \\ B \end{bmatrix} = \begin{bmatrix} I_{RGB}(F_R, 0, 0) \\ I_{RGB}(0, R_G, 0) \\ I_{RGB}(0, 0, R_B) \end{bmatrix} \qquad (6)$$

After splitting the RGB image into three streams, it was converted to the YUV format using the following formula.

$$\begin{bmatrix} Y \\ U \\ V \end{bmatrix} = \begin{bmatrix} 0.299 & 0.587 & 0.114 \\ -0.14713 & -0.28886 & 0.436 \\ 0.615 & -0.51499 & -0.10001 \end{bmatrix} \begin{bmatrix} R \\ G \\ B \end{bmatrix} \qquad (7)$$

Thus, the color wavelet difference reduction (CWDR) algorithm follows the basic concepts of WDR [56] by incorporating extra features that aggregate the coefficients to an area of interest. It is suitable for compressing medical images at a low bit rate per pixel.

Algorithm 2 : The CWDR Algorithm

Input: Original uncompressed image.

1: Convert to YUV- Divide into three streams.
2: **for all** streams **do**
3:    Calculate the DWT of the stream.
4:    **while** (Predetermined number of bits is not reached) **do**
5:       Sort the wavelet transform coefficients from the larger scale to the finer scale.
6:       Set an initial threshold: $T_n = 2^N$, where $N = \log_2(\max_{(i,j)} \vee \gamma(i,j))$, with $n = 1$, where $\gamma(i,j)$ are the wavelet coefficients in the set of non-significant coefficients and N is the total number of bit planes.
7:       Sorting pass: Find the positions of the significant coefficients concerning the threshold, and keep the coefficients that satisfy the condition: $\gamma(i,j) \geq T_n$.
8:       Improvement process: Get the improvement rates of all significant coefficients, except those found in the sorting pass step of the current iteration.
9:       Update threshold: $n = n + 1$; $T_{n-1} = T_n$; $T_n = \frac{T_n}{2}$
10:   **end while**
11: **end for**
12: Combine three streams.

Output: Compressed image.

After the WDR process, we converted the YUV image back to RGB, using the following formula:

$$\begin{bmatrix} R \\ G \\ B \end{bmatrix} = \begin{bmatrix} 1.164 & 0 & 1.596 \\ 1.164 & -0.392 & -0.813 \\ 1.164 & 2.017 & 0 \end{bmatrix} \begin{bmatrix} Y \\ U \\ V \end{bmatrix} \tag{8}$$

Finally, we combined the three streams back into one RGB image. To combine the three streams into an RGB image, we save them to one variable, a.k.a.:

$$RGB = I(R, G, B) \tag{9}$$

VII. EVALUATION METRICS

The PSNR, SSIM, and compression ratio (CR) were computed to evaluate the results [57].

A. PSNR

PSNR computes the peak signal-to-noise ratio between two images in decibels (dB). This ratio is a quality measurement between the original and the compressed image. PSNR can take values up to infinity; the higher the PSNR, the better the compressed image quality. Since the MRI exams in the TCIA dataset contain 16-bit images, in this case, the PSNR is computed as [58]:

$$PSNR = 10 \log_{10} \left(\frac{(2^{16} - 1)^2}{MSE} \right) \tag{10}$$

where $MSE = \frac{\sum_{i=0}^{N-1} \sum_{j=0}^{M-1} (x(i,j) - \hat{x}(i,j))^2}{NM}$, with $x(i,j)$ and $\hat{x}(i,j)$ correspond to the pixel value at position (I, j) of the ground truth x (original uncompressed image) and the compressed

image $\hat{x}$ of dimensions $N \times M$, respectively. Note that the term $2^{16} - 1$ is the maximum pixel value in the input image data type. Since our images have three channels, PSNR is calculated for each channel separately, and the total PSNR is calculated as follows:

$$PSNR = \frac{PSNR_R + PSNR_G + PSNR_B}{3} \tag{11}$$

B. SSIM

SSIM is a metric that represents a visual distortion between a reference image and the observed/compressed image. The SSIM is a function between two images x, and $\hat{x}$ and is computed between pairs of local square overlapping windows x and $\hat{x}$ of the two images [58]. The SSIM calculation is defined in the formula (12).

$$SSIM(x, \hat{x}) = \frac{(2\mu_x \mu_{\hat{x}} + C_1)(2\sigma_{x\hat{x}} + C_2)}{(\mu_x^2 + \mu_{\hat{x}}^2 + C_1)(\sigma_x^2 + \sigma_{\hat{x}}^2 + C_2)} \tag{12}$$

Since the images used in the experimental part have three channels, SSIM is calculated for each channel separately, and the total SSIM is calculated using the formula in (13).

$$SSIM = \frac{SSIM_R + SSIM_G + SSIM_B}{3} \tag{13}$$

C. CR

The CR is defined in equation (14) as the original image's bitstream to the compressed image's bitstream ratio [58].

$$CR = \frac{Total\ bits\ in\ original.\ image}{Total\ bits\ in\ compressed\ image} \tag{14}$$

VIII. RESULTS

The proposed method is evaluated in the demanding field of histopathological microscopy image analysis. The diagnosis and prognosis systems based on histological image analysis present significant growth during the last five years, utilizing whole slide scanning technologies, computational resources management, distributed systems, and multiple cores. According to the medical question, histological microscopy images are extracted using standard tissue preparation procedures. The employed dataset has been extracted using the Hamamatsu NanoZoomer 210, scanning 31 slides of colorectal cancer. The scanning system provides two optical magnification options ($20\times$ and $40\times$), which can scan 210 slides automatically. According to digitalization, each pixel of a Whole Slide Image (WSI) corresponds to a physical area of several tens of nm^2.

Specifically, in $40\times$ magnification mode, the Hamamatsu NanoZoomer scanner extracts an image where the size of each pixel edge corresponds to 227 nm. The above image digitization procedure provides an appropriate resolution for most histological findings. In most cases, the extracted images are stored in compressed JPEG-based or uncompressed TIFF format. The resolution of a typical WSI in $40\times$ magnification is about 100K $\times$ 100K pixels, whereas an uncompressed format could require hundreds of GBs of memory. Commonly, the challenge of compressing images

TABLE 1. Evaluation of CWDR model in terms of PSNR and SSIM for the 31 images.

	Image	PSNR	SSIM
	1768-18TH_1	41.1934	0.9473
	1870-18H_1	47.2838	0.9308
	1870-18H_2	45.1102	0.9344
	1870-18H_3	33.6743	0.9393
	1884-1921_1	36.2088	0.8996
	2529-20H_1	37.6522	0.9316
	2529-20TH_1	37.6522	0.9220
	3211-20AH_1	37.8373	0.9245
	3211-20B_1	36.3347	0.9200
	3469-18H_1	45.7910	0.9300
	4015-14F_1	45.0333	0.9268
	4015-14L_1	44.4740	0.9369
	4339-20N_1	38.9031	0.9311
	4339-20X_1	37.1588	0.9300
	5820-14N_1	47.4880	0.9333
Bit Rate 0.5 CR= 16	5820-14I_1	45.1940	0.9288
	6448-19MX_1	35.8616	0.9300
	7438-16C_1	44.5228	0.9583
	7438-16D_1	43.8831	0.9600
	7870-18A_1	46.3653	0.9400
	7995-17DK_1	45.3092	0.9300
	8036-1BK_1	42.5244	0.9401
	8036-1BK_2	41.8953	0.9288
	8036-1BK_3	42.6988	0.9377
	8036-1BK_4	42.8339	0.9384
	8036-1BK_5	42.6134	0.9391
	8036-1BP_1	43.3838	0.9330
	8036-1BP_2	41.9381	0.9292
	8036-1BP_3	40.7767	0.9404
	8036-1BP_4	41.7617	0.9292
	8036-1BP_5	45.7987	0.9299

FIGURE 5. PSNR values of the 31 images. This figure depicts the PSNR values for all 31 images. It can be seen that the proposed CWDR method managed to achieve values over 30 in all cases, which indicates very good results. Additionally, 74.19% of the cases got an even higher PSNR value (> 40), indicating excellent image quality.

FIGURE 6. SSIM values of the 31 images. This figure depicts the SSIM values for all 31 images. It can be seen that the proposed CWDR method managed to achieve values very close to 1 in 30 out of 31 cases which indicates that the compressed images are completely the same as the original uncompressed ones.

focuses on image size minimization, along with the high performance of quality measures (Signal to Noise Ratio - SNR, Peak Signal to Noise Ratio - PSNR, Structural Similarity – SSIM). However, the most significant issue for histological microscopy images must be the image quality assessment of the medical regions of interest, such as cells and nuclei, cell degeneration and cancer, inflammation and fibrosis areas, and other histological lesions. For the above reason, parts from each WSI after applying the compression procedure, were extracted for evaluation by a specialist.

Table 1, Fig. 5, and Fig. 6 show the results in terms of PSNR and SSIM for the 31 images of our dataset using the CWDR algorithm at a bit rate of 0.5 bit per pixel, which gives a compression ratio of 16. It can be seen that PSNR varies from 32,01 to 47,49. On the other hand, SSIM varies from 0,68 to 0,98, with 30 out of 31 images having an SSIM value of 0,92 or higher.

PSNR values over 30 indicate a very good image quality, and values over 40 indicate that the image quality is excellent (i.e., very close to the original image). It can be seen that the proposed method gives auspicious results since 23 out of 31 images have PSNR values over 40.

Additionally, SSIM values are close to the absolute 1 (which implies that the two images are entirely the same), further supporting the promising results of our method.

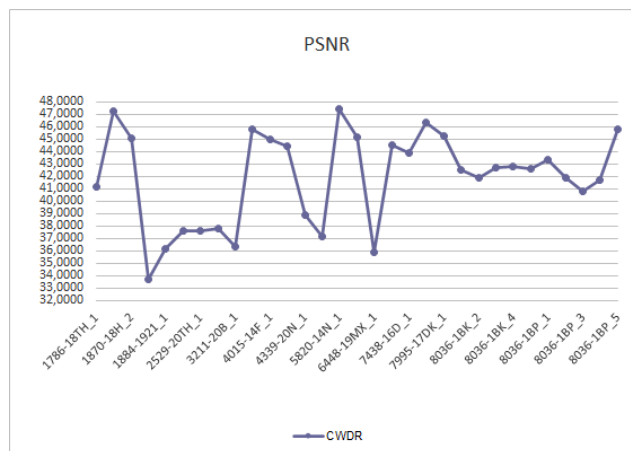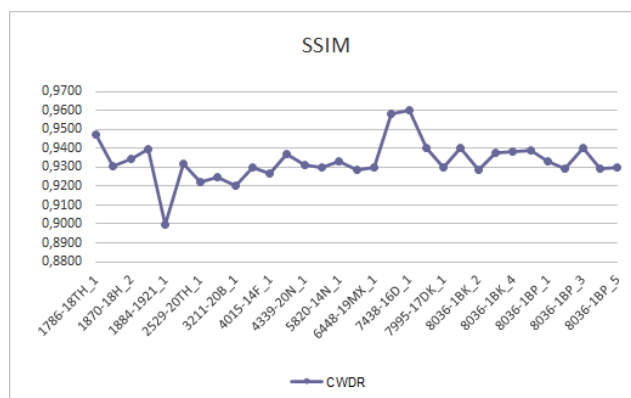The Wilcoxon signed-rank test was used to compare the PSNR values of the proposed method with the respective values for DWT, JPEG 2000, HEIC (high-efficiency image format) and WEBP (web picture format) methods. High-Efficiency Image File Format is a container format for storing individual digital images and image sequences. The standard covers multimedia files that can also include other media streams, such as timed text, audio and video. WEBP is a modern image format that provides superior lossless and lossy compression for images on the web. The Wilcoxon signed-rank test is a non-parametric statistical hypothesis test used either to test the location of a population based on a sample of data or to compare the locations of two populations using two matched samples. The results obtained with those statistical tests are shown in Fig. 7 and indicated statistically significant differences between the CWDR and the other four methods.

We also compared the SSIM values of the proposed method with the respective values for Lossless Compressing Using
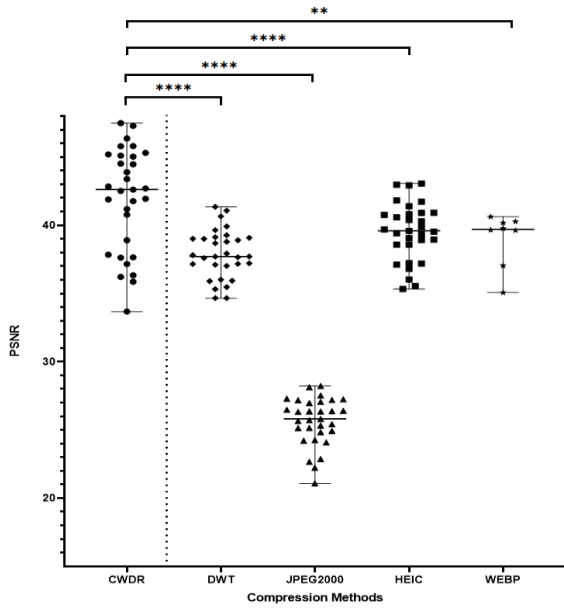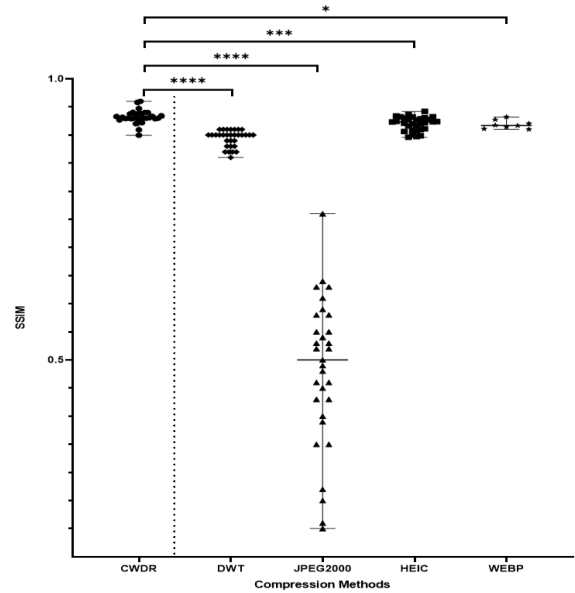
FIGURE 7. Scatter plot representation and the Wilcoxon signed-rank test results of the comparison for each of the two well-known compression methods (Lossless Compressing Using DWT Technique [59], JPEG 2000, HEIC and WEBP) with the CWDR method regarding PSNR values. Stars links join significantly different values; three stars (***) stand for $p < 0.001$, which means that if the null hypothesis tested were indeed true, there would be a one in 1,000 chance of observing results at least as extreme.

FIGURE 8. Scatter plot representation and the Wilcoxon signed-rank test results of the comparison for each of the two compression methods (Lossless Compressing Using DWT Technique [59], JPEG 2000, HEIC and WEBP) with the CWDR method regarding the SSIM values. Stars links join significantly different values; three stars (***) stand for $p < 0.001$.

DWT Technique [59], JPEG 2000, HEIC, and WEBP methods using the Wilcoxon signed-rank test. The results obtained with those statistical tests are shown in Fig. 8 and indicated statistically significant differences between the CWDR and the other four methods.

It should be noted that the images that WEBP method can compress are limited to 16383 pixels in height and width. Therefore, we could only compress 16 out of our 31 images. It can be seen in Fig. 9, and Fig. 10, that the decoded images maintain all the diagnostically important information. Thus, they can be considered as "visually and diagnostically lossless." Even in Fig. 10, which depicts the results of the image with the worst SSIM value (image 1870-18H_3), the result is visually and diagnostically lossless.

IX. DISCUSSION

The proposed method is evaluated in the demanding field of histopathological microscopy image analysis. Utilizing the advantages of whole slide scanning technologies, computational resources management, distributed systems, and multiple cores, the diagnosis and prognosis systems based on histological image analysis presented significant growth during the last five years. Histological microscopy images are extracted after standard tissue preparation procedures. The employed dataset has been extracted using the Hamamatsu NanoZoomer 210, which scanned 31 slides of colorectal cancer. The scanning system provides two optical magnification options (20× and 40×), which can scan 210 slides
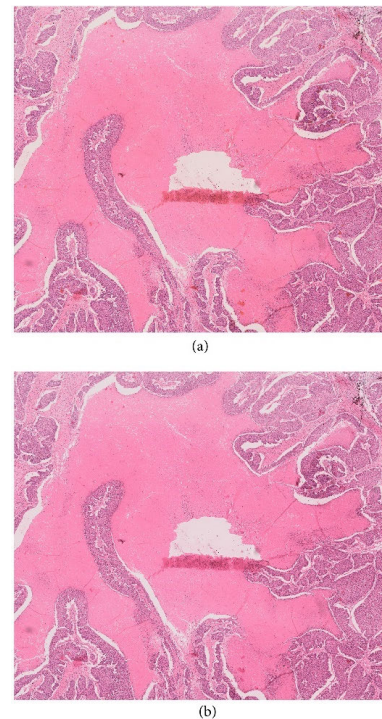

FIGURE 9. 7438-16D_1: (a) Original uncompressed image and (b) compressed image using the CWDR method for compression. It can be seen from both images that they are visually and diagnostically lossless.

automatically. According to digitization, each pixel of a whole slide image (WSI) corresponds to a physical area of several tens of nm^2. Specifically, in 40× magnification mode, the Hamamatsu NanoZoomer scanner extracts an image
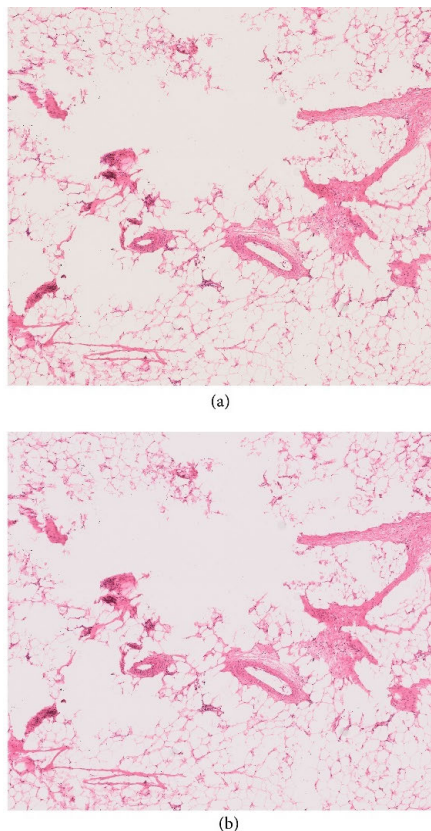
(a)

(b)

FIGURE 10. 1870-18H_3: (a) Original uncompressed image and (b) compressed image using the CWDR method for compression. It can be seen from both images that they are visually and diagnostically lossless.

where the size of each pixel edge corresponds to 227 *nm*. Such image digitization provides appropriate resolution for most histological findings. In most cases, the extracted images are stored in compressed JPEG-based or uncompressed TIFF format. The resolution of a typical WSI in $40\times$ magnification is about 100K $\times$ 100K pixels, which uncompressed format could require hundreds of GBs of memory. Commonly, the challenge of compressing images focuses on image size minimization, along with a high performance of quality measures (SNR, PSNR, and SSIM). However, the most significant issue for histological microscopy images must be the image quality assessment of the medical regions of interest, such as cells and nuclei, cell degeneration and cancer, inflammation and fibrosis areas, and other histological lesions. Due to this, after applying the compression procedure, parts from each WSI have been extracted for evaluation by a specialist.

The perceived quality of the compressed images was evaluated with a Mean Opinion Score (MOS) scale ranging from 1 to 5 (bad, poor, fair, good, and excellent). Even though its suitability may be debatable, the MOS scale provides a different method of gauging the quality and depicting how specialists evaluates it [60]. Four qualified histopathologists evaluated the quality of the compressed images without blindly consulting each other. The proposed compression method met high qualitative criteria obtaining similar image
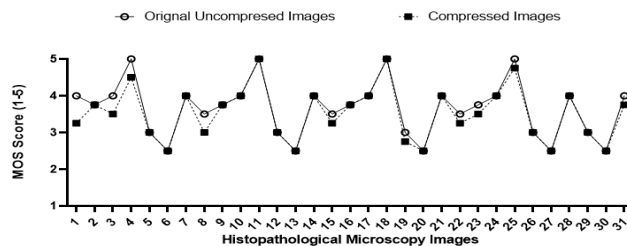

FIGURE 11. Spearman's rank-order correlations were to examine the association between the MOS score of original uncompressed images and compressed images using the proposed method. There were positive and significant associations between the two MOS scores, ($r_s = 0.9539$, $N = 31$, $p < 0.001$).

quality rating score, with a statistically significant association comparing to original uncompressed images (Fig. 11).

X. CONCLUSION

The purpose behind extending the original WDR method for color images was to create an easily reproducible compression method for large-size medical images. Specifically, extensive evaluations have been performed in a custom-created dataset containing 31 slides on colorectal cancer. It achieved state-of-the-art compression results with a high compression ratio and slight information loss within an acceptable range. The image quality was evaluated using the MOS scale, where four qualified histopathologists verified that the compressed images met highly qualitative criteria. The statistical significance of the proposed method was compared with four compression algorithms (DWT Technique, JPEG 2000, HEIC and WEBP) using the Wilcoxon signed-rank test. The statistical test's outcome found significant differences between the proposed algorithm and the other four compression methods. Future work includes implementing a mobile and web platform that may be used to compress and transmit medical images in real time.

REFERENCES

[1] R. Duszak and L. Harvey, "Medical imaging: Is the growth boom over?" Neiman Health Policy Inst., Reston, VA, USA, Tech. Rep. 1, 2012.

[2] A. J. Hussain, A. Al-Fayadh, and N. Radi, "Image compression techniques: A survey in lossless and lossy algorithms," *Neurocomputing*, vol. 300, pp. 44–69, Jul. 2018.

[3] R. Leung and D. Taubman, "Transform and embedded coding techniques for maximum efficiency and random accessibility in 3-D scalable compression," *IEEE Trans. Image Process.*, vol. 14, no. 10, pp. 1632–1646, Oct. 2005.

[4] N. Ahmed, "How I came up with the discrete cosine transform," *Digit. Signal Process.*, vol. 1, no. 1, pp. 4–5, Jan. 1991.

[5] V. Britanak, P. C. Yip, and K. R. Rao, *Discrete Cosine and Sine Transforms: General Properties, Fast Algorithms and Integer Approximations*. Amsterdam, The Netherlands: Elsevier, 2010.

[6] P. Schelkens, A. Munteanu, J. Barbarien, M. Galca, X. Giro-Nieto, and J. Cornelis, "Wavelet coding of volumetric medical datasets," *IEEE Trans. Med. Imag.*, vol. 22, no. 3, pp. 441–458, Mar. 2003.

[7] C. Narmatha, P. Manimegalai, and S. Manimurugan, "A lossless compression scheme for grayscale medical images using a P2-bit short technique," *J. Med. Imag. Health Informat.*, vol. 7, no. 6, pp. 1196–1204, Oct. 2017.

[8] H. Amri, A. Khalfallah, M. Gargouri, N. Nebhani, J.-C. Lapayre, and M.-S. Bouhlel, "Medical image compression approach based on image resizing, digital watermarking and lossless compression," *J. Signal Process. Syst.*, vol. 87, no. 2, pp. 203–214, 2017.

[9] T. Bruylants, A. Munteanu, and P. Schelkens, "Wavelet based volumetric medical image compression," *Signal Process. Image Commun.*, vol. 31, pp. 112–133, Feb. 2015.

[10] D. Ravichandran, M. G. Ahamad, and M. R. A. Dhivakar, "Performance analysis of three-dimensional medical image compression based on discrete wavelet transform," in *Proc. 22nd Int. Conf. Virtual Syst. Multimedia (VSMM)*, Oct. 2016, pp. 1–8.

[11] R. K. Senapati, P. M. K. Prasad, G. Swain, and T. N. Shankar, "Volumetric medical image compression using 3D listless embedded block partitioning," *SpringerPlus*, vol. 5, no. 1, pp. 1–16, Dec. 2016.

[12] X. Tang and W. A. Pearlman, "Three-dimensional wavelet-based compression of hyperspectral images," in *Hyperspectral Data Compression*, G. Motta, F. Rizzo, and J. A. Storer, Eds. Boston, MA, USA: Springer, 2006, doi: 10.1007/0-387-28600-4_10.

[13] Z. Chen, S. Gu, G. Lu, and D. Xu, "Exploiting intra-slice and inter-slice redundancy for learning-based lossless volumetric image compression," *IEEE Trans. Image Process.*, vol. 31, pp. 1697–1707, 2022.

[14] O. H. Nagoor, J. Whittle, J. Deng, B. Mora, and M. W. Jones, "Lossless compression for volumetric medical images using deep neural network with local sampling," in *Proc. IEEE Int. Conf. Image Process. (ICIP)*, Oct. 2020, pp. 2815–2819.

[15] M. C. Zerva, M. Vrigkas, L. P. Kondi, and C. Nikou, "Improving 3D medical image compression efficiency using spatiotemporal coherence," *Electron. Imag.*, vol. 2020, no. 10, pp. 1–63, 2020.

[16] L. F. R. Lucas, N. M. M. Rodrigues, L. A. da Silva Cruz, and S. M. M. de Faria, "Lossless compression of medical images using 3-D predictors," *IEEE Trans. Med. Imag.*, vol. 36, no. 11, pp. 2250–2260, Nov. 2017.

[17] A. AbuBaker, M. Eshtay, and M. AkhoZahia, "Comparison study of different lossy compression techniques applied on digital mammogram images," *Int. J. Adv. Comput. Sci. Appl.*, vol. 7, no. 12, pp. 149–155, 2016.

[18] G. K. Wallace, "The JPEG still picture compression standard," *IEEE Trans. Consum. Electron.*, vol. 38, no. 1, pp. 18–34, Feb. 1992.

[19] M. Rabbani and R. Joshi, "An overview of the JPEG 2000 still image compression standard," *Signal Process., Image Commun.*, vol. 17, no. 1, pp. 3–48, Jan. 2002.

[20] Q. Cai, L. Song, G. Li, and N. Ling, "Lossy and lossless intra coding performance evaluation: HEVC, H.264/AVC, JPEG 2000 and JPEG LS," in *Proc. Asia Pacific Signal Inf. Process. Assoc. Annu. Summit Conf.*, Dec. 2012, pp. 1–9.

[21] D. A. Huffman, "A method for the construction of minimum-redundancy codes," *Proc. IRE*, vol. 40, no. 9, pp. 1098–1101, Sep. 1952.

[22] G. G. Langdon, "An introduction to arithmetic coding," *IBM J. Res. Develop.*, vol. 28, no. 2, pp. 135–149, Mar. 1984.

[23] J. W. McCoy, N. Magotra, and S. Stearns, "Lossless predictive coding," in *Proc. 37th Midwest Symp. Circuits Syst.*, vol. 2, 1994, pp. 927–930.

[24] D. Dube, "Lossless compression of grayscale and colour images using multidimensional CSE," in *Proc. 11th Int. Symp. Image Signal Process. Anal. (ISPA)*, Sep. 2019, pp. 222–227.

[25] V. Makarichev, V. Lukin, and I. Brysina, "Lossless discrete atomic compression of full color digital images," in *Proc. IEEE 16th Int. Conf. Exper. Designing Appl. CAD Syst. (CADSM)*, Feb. 2021, pp. 43–46.

[26] J. Lee, J. Yun, J. Lee, I. Hwang, D. Hong, Y. Kim, C. G. Kim, and W.-C. Park, "An effective algorithm and architecture for the high-throughput lossless compression of high-resolution images," *IEEE Access*, vol. 7, pp. 138803–138815, 2019.

[27] A. Descampe, T. Richter, T. Ebrahimi, S. Foessel, J. Keinert, T. Bruylants, P. Pellegrin, C. Buysschaert, and G. Rouvroy, "JPEG XS—A new standard for visually lossless low-latency lightweight image coding," *Proc. IEEE*, vol. 109, no. 9, pp. 1559–1577, Sep. 2021.

[28] Q. Min, X. Wang, B. Huang, and Z. Zhou, "Lossless medical image compression based on anatomical information and deep neural networks," *Biomed. Signal Process. Control*, vol. 74, Apr. 2022, Art. no. 103499.

[29] F. Yang, J. Mou, K. Sun, and R. Chu, "Lossless image compression-encryption algorithm based on BP neural network and chaotic system," *Multimedia Tools Appl.*, vol. 79, nos. 27–28, pp. 19963–19992, Jul. 2020.

[30] H. Rhee, Y. I. Jang, S. Kim, and N. I. Cho, "Lossless image compression by joint prediction of pixel and context using duplex neural networks," *IEEE Access*, vol. 9, pp. 86632–86645, 2021.

[31] C. Zhu, H. Zhang, and Y. Tang, "Lossless image compression algorithm based on long short-term memory neural network," in *Proc. 5th Int. Conf. Comput. Intell. Appl. (ICCIA)*, Jun. 2020, pp. 82–88.

[32] A. Al-Fayadh, A. J. Hussain, P. Lisboa, and D. Al-Jumeily, "Hybrid classified vector quantisation and its application to image compression," in *Proc. Int. Conf. 'Comput. Tool' (EUROCON)*, 2007, pp. 157–162.

[33] K. R. Rao and P. C. Yip, Eds., *The Transform and Data Compression Handbook*, 1st ed. Boca Raton, FL, USA: CRC Press, 2001, doi: 10.1201/9781315220529.

[34] K. Karhunen, "On linear methods in probability theory," *Annales Academiae Scientiarum Fennicae*, vol. 47, 1947.

[35] M. Loeve, "Functions aleatoires du second ordre," *Processus stochastique et mouvement Brownien*, pp. 366–420, 1948.

[36] G. Anderson and T. Huang, "Piecewise Fourier transformation for picture bandwidth compression," *IEEE Trans. Commun.*, vol. COM-19, no. 2, pp. 133–140, Apr. 1971.

[37] K. G. Beauchamp, *Applications of Walsh and Related Functions, With an Introduction to Sequency Theory*, vol. 2. New York, NY, USA: Academic, 1984.

[38] T. Beer, "Walsh transforms," *Amer. J. Phys.*, vol. 49, no. 5, pp. 466–472, 1981.

[39] P. S. Addison, "Wavelet transforms and the ECG: A review," *Physiol. Meas.*, vol. 26, no. 5, pp. R155–R199, Oct. 2005.

[40] S. Xu, J. Zhang, L. Bo, H. Li, H. Zhang, Z. Zhong, and D. Yuan, "Singular vector sparse reconstruction for image compression," *Comput. Electr. Eng.*, vol. 91, May 2021, Art. no. 107069.

[41] L. Guo, D. Zhou, J. Zhou, S. Kimura, and S. Goto, "Lossy compression for embedded computer vision systems," *IEEE Access*, vol. 6, pp. 39385–39397, 2018.

[42] A. Sadchenko, O. Kushnirenko, and O. Plachinda, "Fast lossy compression algorithm for medical images," in *Proc. Int. Conf. Electron. Inf. Technol. (EIT)*, May 2016, pp. 1–4.

[43] Y. Dua, R. S. Singh, K. Parwani, S. Lunagariya, and V. Kumar, "Convolution neural network based lossy compression of hyperspectral images," *Signal Process., Image Commun.*, vol. 95, Jul. 2021, Art. no. 116255.

[44] L. Zhao, H. Bai, A. Wang, and Y. Zhao, "Multiple description convolutional neural networks for image compression," *IEEE Trans. Circuits Syst. Video Technol.*, vol. 29, no. 8, pp. 2494–2508, Aug. 2019.

[45] D. Mishra, S. K. Singh, and R. K. Singh, "Lossy medical image compression using residual learning-based dual autoencoder model," in *Proc. IEEE 7th Uttar Pradesh Sect. Int. Conf. Electr., Electron. Comput. Eng. (UPCON)*, Nov. 2020, pp. 1–5.

[46] R. M. Slone, D. H. Foos, B. R. Whiting, E. Muka, D. A. Rubin, T. K. Pilgram, K. S. Kohm, S. S. Young, P. Ho, and D. D. Hendrickson, "Assessment of visually lossless irreversible image compression: Comparison of three methods by using an image-comparison workstation," *Radiology*, vol. 215, no. 2, pp. 543–553, May 2000.

[47] B. J. Erickson, "Irreversible compression of medical images," *J. Digit. Imag.*, vol. 15, no. 1, pp. 5–14, Mar. 2002.

[48] S. Krivenko, V. Lukin, O. Krylova, L. Kryvenko, and K. Egiazarian, "A fast method of visually lossless compression of dental images," *Appl. Sci.*, vol. 11, no. 1, p. 135, Dec. 2020.

[49] Z. Wang, A. C. Bovik, H. R. Sheikh, and E. P. Simoncelli, "Image quality assessment: From error visibility to structural similarity," *IEEE Trans. Image Process.*, vol. 13, no. 4, pp. 600–612, Apr. 2004.

[50] N. Ponomarenko, V. Lukin, J. Astola, and K. Egiazarian, "Analysis of HVS-metrics' properties using color image database TID2013," in *Proc. 16th Int. Conf. Adv. Concepts Intell. Vis. Syst. (ACIVS)*, vol. 9386. Berlin, Germany: Springer-Verlag, 2015, pp. 613–624, doi: 10.1007/978-3-319-25903-1_53.

[51] K. J. Balakrishnan and N. A. Touba, "Relationship between entropy and test data compression," *IEEE Trans. Comput.-Aided Design Integr. Circuits Syst.*, vol. 26, no. 2, pp. 386–395, Feb. 2007.

[52] A. Zemliachenko, V. Lukin, N. Ponomarenko, K. Egiazarian, and J. Astola, "Still image/video frame lossy compression providing a desired visual quality," *Multidimensional Syst. Signal Process.*, vol. 27, no. 3, pp. 697–718, Jul. 2016.

[53] H. L. Resnikoff and R. O. Wells, *Wavelet Analysis: The Scalable Structure of Information*, 1st ed. Berlin, Germany: Springer-Verlag, Sep. 1998, p. XVI and 435, doi: 10.1007/978-1-4612-0593-7.

[54] J. Walker and T. Q. Nguyen, "Wavelet-based image compression," in *Handbook of Transforms and Data Compression*. 2001, ch. 6, pp. 267–312.

[55] T. Sultana, "Image compression technique WDR and EZW for different wavelet codes," *J. Multimedia Process. Technologie*, vol. 6, no. 2, pp. 43–52, 2015.

[56] X. Wu and N. Memon, "Context-based, adaptive, lossless image coding," *IEEE Trans. Commun.*, vol. 45, no. 4, pp. 437–444, Apr. 1997.

[57] I. Blanes, J. Serra-Sagristà, M. W. Marcellin, and J. Bartrina-Rapesta, "Divide-and-conquer strategies for hyperspectral image processing: A review of their benefits and advantages," *IEEE Signal Process. Mag.*, vol. 29, no. 3, pp. 71–81, May 2021.

[58] S. Raja and A. Suruliandi, "Image compression using WDR & ASWDR techniques with different wavelet codecs," *ACEEE Int. J. Inf. Technol.*, vol. 1, pp. 23–26, Sep. 2011.

[59] F. Grillo and J. Balbás, "Lossless compressing usin DWT tecnique," MATLAB Central File, 2020. [Online]. Available: https://www.mathworks.com/matlabcentral/fileexchange/81308-lossless-compression-using-dwt-tecnique?s_tid=FX_rc1_behav

[60] Q. Huynh-Thu, M.-N. Garcia, F. Speranza, P. Corriveau, and A. Raake, "Study of rating scales for subjective quality assessment of high-definition video," *IEEE Trans. Broadcast.*, vol. 57, no. 1, pp. 1–14, Mar. 2011.

MATINA C. H. ZERVA was born in Greece, in 1989. She received the B.Sc. degree in computer science from the Department of Computer Science and Engineering and the M.Sc. degree in applied mathematics and computer science from the Department of Mathematics. She is currently pursuing the Ph.D. degree with the Department of Computer Science and Engineering, University of Ioannina, Greece, where she is a Researcher with the Department of Computer Science and Engineering. She works as a computer teacher in a private computer school she owns. Her main research interests include medical images compression and enhancement.

VASILEIOS CHRISTOU received the B.Sc. degree from the Telematics and Administration Department, Technological Educational Institute of Epirus, Greece, in 2008, the M.Sc. degree in technology of education and digital systems from the University of Piraeus, Greece, in 2012, and the Ph.D. degree in machine learning from the University of Manchester, U.K., in 2019. He is currently a Researcher with the University of Ioannina, Greece. His research interests include evolutionary computing, extreme learning machine, and deep learning.
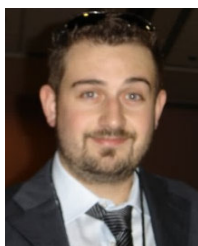
NIKOLAOS GIANNAKEAS received the dual B.Sc. degree in physics and computer science from the University of Ioannina, Greece, and Hellenic Open University, Greece, respectively, and the Ph.D. Diploma degree in bioinformatics from the Medical School, University of Ioannina, where he has been an Assistant Professor in signal and systems with the Informatics and Telecommunications Department, since 2019. He was worked for more than 15 years in research projects funded by National and European Programs (3rd CSF, NSRF 2007–2013, NSRF 2014–2020, FP6, FP7, and Horizon 2020). He has published more than 100 international journals, conference proceedings, and book chapters. His research interests include signal processing and image analysis, artificial intelligence and machine learning, bioinformatics, and biomedical engineering.

ALEXANDROS T. TZALLAS received the B.Sc. degree in physics and the Ph.D. degree in medical physics from the University of Ioannina, Ioannina, Greece, in 2001 and 2009, respectively. He holds a position as an Associate Professor in biomedical engineering and specifically in analysis and processing of biomedical data with the Department of Informatics and Telecommunications, University of Ioannina, Arta, Greece. He is also affiliated as an Academic Research Fellow at several Research and Technology Institutes, Greece, and the U.K. His research interests include neuroscience, electroencephalography, wearable devices, biomedical signal and image processing, biomedical engineering, decision support medical systems, and biomedical applications.

LISIMACHOS P. KONDI (Senior Member, IEEE) received the Diploma degree in electrical engineering from the Aristotle University of Thessaloniki, Greece, in 1994, and the M.S. and Ph.D. degrees in electrical and computer engineering from Northwestern University, Evanston, IL, USA, in 1996 and 1999, respectively. He was previously with the faculty of the University at Buffalo, The State University of New York, USA. He has held summer appointments at the Naval Research Laboratory, Washington, DC, USA, and the Air Force Research Laboratory, Rome, NY, USA. He is currently a Professor with the Department of Computer Science and Engineering, University of Ioannina, Greece. He is the coauthor of a book titled *4G Wireless Video Communications* (Wiley, 2009). His research interests include the general areas of signal and image processing and communications, image and video compression and transmission over wireless channels and the internet, perceptual image and video quality estimation, sparse representations and compressive sensing, super-resolution of video sequences, and shape coding. He was the Technical Program Committee (TPC) Chair of the International Conference on Digital Signal Processing (DSP), Santorini, Greece, in 2013, and the Technical Program Committee Chair of the IEEE International Conference on Image Processing (ICIP), Athens, Greece, in 2018. He has been an Associate Editor of the *EURASIP Journal on Advances in Signal Processing*, since 2005; the IEEE Transactions on Image Processing, since 2018; the IEEE Signal Processing Letters, from 2008 to 2012; and the *International Journal of Distributed Sensor Networks*, from 2013 to 2015.

• • •